The Journal of Experimental Biology 216, 3071-3083

doi:10.1242/jeb.087742

RESEARCH ARTICLE

Visually guided gradation of prey capture movements in larval zebrafish

Bradley W. Patterson[1], Aliza O. Abraham[2], Malcolm A. MacIver[1,2,3,4,*] and David L. McLean[1,4,*]

[1]Interdepartmental Neuroscience Program, Northwestern University, Evanston, IL, USA, [2]Department of Mechanical Engineering, Northwestern University, Evanston, IL, USA, [3]Department of Biomedical Engineering, Northwestern University, Evanston, IL, USA and [4]Department of Neurobiology, Northwestern University, Evanston, IL, USA

*Authors for correspondence (maciver@northwestern.edu; david-mclean@northwestern.edu)

SUMMARY

A mechanistic understanding of goal-directed behavior in vertebrates is hindered by the relative inaccessibility and size of their nervous systems. Here, we have studied the kinematics of prey capture behavior in a highly accessible vertebrate model organism, the transparent larval zebrafish (*Danio rerio*), to assess whether they use visual cues to systematically adjust their movements. We found that zebrafish larvae scale the speed and magnitude of turning movements according to the azimuth of one of their standard prey, paramecia. They also bias the direction of subsequent swimming movements based on prey azimuth and select forward or backward movements based on the prey's direction of travel. Once within striking distance, larvae generate either ram or suction capture behaviors depending on their distance from the prey. From our experimental estimations of ocular receptive fields, we ascertained that the ultimate decision to consume prey is likely a function of the progressive vergence of the eyes that places the target in a proximal binocular 'capture zone'. By repeating these experiments in the dark, we demonstrate that paramecia are only consumed if they contact the anterior extremities of larvae, which triggers ocular vergence and tail movements similar to close proximity captures in lit conditions. These observations confirm the importance of vision in the graded movements we observe leading up to capture of more distant prey in the light, and implicate somatosensation in captures in the absence of light. We discuss the implications of these findings for future work on the neural control of visually guided behavior in zebrafish.

Supplementary material available online at http://jeb.biologists.org/cgi/content/full/216/16/3071/DC1

Key words: kinematics, visuomotor integration, *Danio rerio*, behavior.

Received 4 March 2013; Accepted 15 April 2013

INTRODUCTION

Visually guided behaviors rely on the appropriate translation of photons into actions. While we understand much about the sensory neurons that respond to light (Borst, 2009; Masland, 2012; Sanes and Zipursky, 2010) and the motor neurons that generate movements (Brownstone and Stuart, 2011; Jessell et al., 2011; Landgraf and Thor, 2006), less is known about the intermediate steps that enable appropriate responses to visual cues. In vertebrates, a major obstacle to progress is the distributed location and relative inaccessibility of neurons at various stages of visuomotor processing. To gain a greater understanding of visually guided behavior, ideally one would assess the activity and connectivity of cells from photoreceptor to muscle fiber in an intact, behaving animal. The larval zebrafish provides this opportunity.

After only 4–5 days of development, zebrafish larvae can actively forage for food and avoid predation. These abilities rely on rapidly assembled visual and motor networks, whose relative simplicity and optical transparency make them readily amenable to investigation (McLean and Fetcho, 2008; Nikolaou and Meyer, 2012). Although assessments of zebrafish retinal and/or tectal networks *versus* reticular and/or spinal networks are usually performed independently, more recent work has begun to bridge the visual and motor control fields. For example, drifting gratings have been used to reveal the reticulospinal circuitry responsible for asymmetric movements (Orger et al., 2008), to confirm the cerebellum's role in processing discrepancies between perceived and expected sensory feedback (Ahrens et al., 2012) and to implicate the dorsal raphe in different states of arousal (Yokogawa et al., 2012).

In the laboratory, larval zebrafish will track and capture paramecia. Larvae presumably rely on vision to capture prey, as the number of paramecia consumed decreases in the dark (Gahtan et al., 2005). Past work has examined the movements generated by larvae during prey capture (Bianco et al., 2011; Borla et al., 2002; McElligott and O'Malley, 2005). However, these studies were primarily focused on evoking prey capture using simulations or distinguishing capture movements from more routine ones, rather than revealing systematic differences in kinematics related to prey location. This last approach could provide important details for uncovering the neural and mechanical mechanisms underlying this crucial survival skill.

Here, we provide a detailed examination of the kinematics of prey capture with this idea in mind. We found that larval zebrafish can systematically bias the speed, intensity and directionality of their movements based on visual cues. Given the known retinotopic organization of the optic tectum (Baier et al., 1996; Niell and Smith, 2005; Stuermer, 1988) and the topographic organization of reticulospinal and spinal networks according to movement strength (Kimura et al., 2006; Kinkhabwala et al., 2011; Koyama et al., 2011; McLean et al., 2007), our observations provide predictions about the interactions between visual, oculomotor and axial networks

during prey capture. These findings should help future studies of the neural control of visually guided behaviors in zebrafish.

MATERIALS AND METHODS

Animals

Experiments were performed using 5–7 day old zebrafish larvae, *Danio rerio* (Hamilton 1822) obtained from a laboratory stock of wild-type adults. At these early stages of development, zebrafish have not yet sexually differentiated and have almost exhausted their embryonic yolk stores. Fish in our custom-fabricated breeding facility (Aquatic Habitats, Beverly, MA, USA) were maintained at 28.5°C in system water (pH 7.3, conductivity 550 μS) on a 14 h:10 h light:dark cycle. Upon fertilization, eggs were transferred to Petri dishes filled with system water (10 eggs per 25 ml dish) that contained paramecia (200 ml^{-1}, see below), and were raised in an incubator under the same conditions. Larvae were transferred to new dishes containing fresh solutions and paramecia on the third and sixth day. If the embryos had not hatched by the end of the second day, they were carefully de-chorionated using fine forceps to give them relatively equal amounts of exposure to paramecia outside the egg. All recordings of behavior were performed at room temperature (~22°C). Animals were treated in accordance with the National Institutes of Health Guide for the Care and Use of Laboratory Animals and experiments were approved by the Northwestern University Institutional Animal Care and Use Committee.

Paramecium preparation

Paramecia were used as a natural prey item to evoke capture behavior in zebrafish larvae (Bianco et al., 2011; Gahtan et al., 2005; McElligott and O'Malley, 2005; Smear et al., 2007). Larvae raised with paramecia performed prey capture behaviors more frequently and with far shorter latencies (<5 min) compared with control larvae (>30 min), although we have not quantified this further. The inspiration to raise the fish with paramecia came from a study demonstrating that prey preferences in cuttlefish can be modified by early prey exposure (Guibé et al., 2010). Paramecia (*P. aurelia*, *P. bursaria* and *P. multimicronucleatum*; Carolina Biological Supply, Burlington, NC, USA) were cultured separately in 1 l containers at 28.5°C for 2–3 weeks. Live paramecia were added to culture media that contained 750 ml distilled water, 0.5 g powdered brewer's yeast (Twinlab, New York, NY, USA) and 10 boiled wheat seeds (Carolina Biological Supply). Cultures were refreshed weekly with 0.2 g powered yeast and five boiled wheat seeds in 50 ml distilled water.

Before paramecia were added to water containing zebrafish, they were cleaned and concentrated following procedures outlined by the Zebrafish International Resource Center (University of Oregon, Eugene, OR, USA). Briefly, 1 liter of paramecium culture (an equal mixture of two to three different paramecium species) was passed through a 105 μm nylon screen filter (Aquatic Eco-Systems, Apopka, FL, USA) to remove large contaminants, followed by a 20 μm nylon screen filter (Aquatic Eco-Systems) to collect the paramecia and filter out smaller contaminants. These paramecia were re-suspended in ~10 ml of system water. The filtration and re-suspension process was repeated 2–3 times, yielding 30–40 ml of concentrated paramecia. It was crucial that paramecium stock solution was free of detritus for high-speed imaging and automated analysis. The concentration of the cleaned paramecium stock solution was measured by sampling 20 μl of the stock solution and counting the number of paramecia. On average, stock solutions contained 1400 paramecia per ml (1394±990 ml^{-1}; N=26). For rearing conditions, stock solutions were diluted to achieve concentrations of ~5000 paramecia per 25 ml dish (i.e. 200 ml^{-1}).

High-speed behavioral recordings

To observe the prey capture behavior of zebrafish larvae, videos were recorded using a high-speed camera (FASTCAM 1024 PCI; Photron, San Diego, CA, USA) attached to a dissection microscope (Stemi-2000; Carl Zeiss Microscopy, Thornwood, NY, USA). Images were collected at 250 frames s^{-1} at 16.25× magnification. This rate was sufficient to film the relatively slow prey capture maneuvers; however, in some experiments we collected images at 500 frames s^{-1} to provide better temporal resolution. Illumination was provided *via* a ring light 7 cm above the stage at 25,000 lx. Illumination at this distance and intensity had no appreciable effect on water temperature (±1°C), as confirmed using a temperature probe (HCC-100A; Dagan, Minneapolis, MN, USA). A dark, high contrast background was angled below the stage to more easily observe the transparent larvae and paramecia. The testing chamber consisted of a 10 mm diameter circular arena sandwiched between two coverslips, which was connected to a small reservoir by a channel (Fig. 1A–C). The reservoir allowed us to add paramecia without disturbing the larvae. Larvae were introduced into the circular arena one at a time and acclimated for 30 min. After this, paramecia from the cleaned stock solution were added to the reservoir. The height of the testing chamber constricted the movements of the larvae to a single focal plane (~2 mm fluid depth), which simplified data collection but did not impede their movements (larvae are just over 0.5 mm in height). Prey capture videos were collected for 2 h following the acclimation period. The data presented here represent 233 active periods of movement (or 'bouts', see below) from 50 successful captures in 17 different wild-type larvae (1–11 capture trials per fish). For analysis of bouts leading up to the capture, the final capture maneuver was not included in the analysis (N=183). Prey capture trials were excluded from analysis if the larvae contacted the edge of the circular arena at any time during the trial.

To observe prey capture in the dark, the ring light suspended above the imaging arena was covered with an infrared (IR) transmittance filter (Kodak Wratten IR filter #87C; Eastman Kodak, Rochester, NY, USA). The filter only permitted wavelengths above 800 nm to pass through, which we can detect using our IR-sensitive camera, but the zebrafish cannot (Nawrocki et al., 1985). In addition, the entire setup was shielded from light using thick black fabric and experiments were conducted in a dark room. Again, IR illumination did not dramatically alter water temperature (±0.5°C). Images in the dark were captured at 60 or 250 frames s^{-1}. Under these conditions, six successful captures and 13 unsuccessful attempts from five different larvae were analyzed (one to five successful and unsuccessful capture trials per fish). Following our IR-illuminated observations, we always confirmed that the larvae could perform visually guided prey capture by testing them again in the light (N=5).

Data analysis

Videos were analyzed using automated tracking software specifically designed to characterize larval zebrafish axial kinematics (Fontaine et al., 2008). The program tracks the outline of the fish using an elastic kinematic model and generates a 51-point midline (Fig. 1D). Larva position was tracked with a spatial resolution of 10 μm in both dimensions. The image plane covered an area of 10×10 mm and images were collected at 1024×1024 pixel resolution. The coordinates of the fish outline were smoothed using wavelet denoising and then used to extract a number of kinematic variables. All measurements were taken in a coordinate frame with the origin at the top left corner of digitized video images, with positive x-

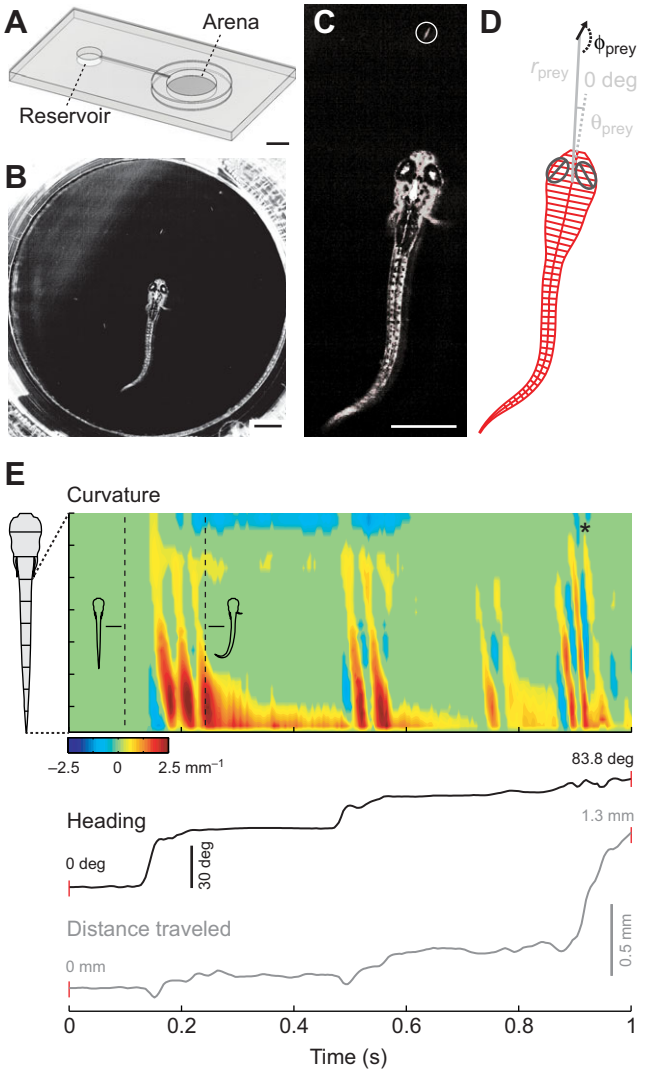

Fig. 1. Collection and analysis of prey capture videos. (A) Diagram of the custom-built testing chamber used for collecting high-speed videos of prey capture behavior. Scale bar, 5 mm. (B) Image of zebrafish larva in the central arena performing prey capture behavior. Scale bar, 1 mm. (C) Enlarged image of the larva from B (note the paramecium in the circle). Scale bar, 1 mm. (D) Information extracted from the image in C following tracking analyses. Red lines indicate the automated processing of axial kinematics whereas black and gray lines indicate the manual measurements of eye and paramecium orientations. The long axes of the eyes are marked by a line bisecting them. Using these data, we could determine the proximity of the paramecium (r_{prey}), its azimuth (θ_{prey}) and its direction of travel (ϕ_{prey}) relative to the fish's body (0 deg reference). (E) A representative trial from a different fish illustrating the curvature of the tail (top panel), the heading of the fish relative to its original heading before detecting the paramecium (middle panel) and the distance traveled (bottom panel) during the entire prey capture sequence. All measurements are presented on the same time scale. In the heat map of curvature, red represents positive values to the left, while blue represents negative values to the right. Outlines of body shape from time points indicated by the dashed lines are included to illustrate this point. The asterisk indicates the point of capture in this sequence.

values extending right and positive *y*-values extending down in the image plane. To examine the angular movement of the head of the fish, a line connecting the center of the head to the center of the swim bladder was used for all measurements. The angle between this line and the positive *x*-axis was computed (θ_{fish}). For other angular values, the magnitude of the fish's movement was represented using a change in angle normalized to the first frame. The angular velocity of the head and its longitudinal velocity were computed using the difference in the tracked head position between successive images. Longitudinal velocity (v_l) was determined using Eqn 1:

$$v_l = v_x \cos\theta_{fish} + v_y \sin\theta_{fish} . \quad (1)$$

Longitudinal acceleration was computed using the difference in the longitudinal velocity between successive velocities as computed above. Body curvature (κ) was calculated using Eqn 2, after taking the first and second derivatives of the *x* and *y* components of the midline down the body of the fish (d*x*, dd*x*, d*y*, dd*y*):

$$\kappa = \frac{dx\ ddy - dy\ ddx}{(dx^2 + dy^2)^{3/2}} . \quad (2)$$

To remove noise from all the curvature data we used a 0.4 mm^{-1} threshold. This threshold was chosen because it was the minimum value that effectively eliminated spurious curvature values as determined by eye. Also, any point rostral to the caudal edge of the swim bladder was set to a curvature of 0 mm^{-1}, as these areas remained straight during body movements, but would occasionally contain a small amount of curvature noise due to pectoral fin movement. We integrated the curvature (symbolized by $\Sigma\kappa$) at the 19% point of the body from the tip of the tail over time as an indirect measure of yaw torque. Positive values represent bends to the left, while negative values represent bends to the right. Tail movement asymmetry (*A*) was normalized to between –1 (maximal rightward integrated curvature) and +1 (maximal leftward integrated curvature) using Eqn 3:

$$A = \frac{\Sigma\kappa}{\Sigma|\kappa|} . \quad (3)$$

To evaluate the final capture movements, we generated a normalized ram–suction index (RSI) score (Eqn 4) (Norton and Brainerd, 1993) by comparing the distance moved by the predator (D_{pred}, caused by ram-type movements) with the distance moved by prey item (D_{prey}, movement caused by suction):

$$RSI_{score} = \frac{D_{pred} - D_{prey}}{D_{pred} + D_{prey}} . \quad (4)$$

To determine the point at which larvae detected paramecia, we tracked back from the point of capture and identified when larvae made their first orientation turn toward the paramecium. All prey capture videos start 120 ms prior to the first orientation movement and were tracked for at least 100 ms following ingestion.

The motion of the larvae consisted of bouts of activity followed by quiescence. We defined the onset of a bout as any movement at or following prey detection as determined by manual inspection of the high-speed video upon playback. Consistent with spontaneous swimming, bouts were typically initiated with bilateral pectoral fin abduction (Green et al., 2011), which occurred either alone or in conjunction with eye movement (Bianco et al., 2011). Complete relaxation of the tail marked the end of the bout. In some cases (4 of 233), bilateral fin abduction initiating a new bout occurred before the tail had completely relaxed. These were still counted as separate bouts, although the interval would be recorded as 0 ms. Tail-beat frequency was measured by taking the reciprocal of the interval between the peak amplitudes of bends. For tail beat frequency, we only measured alternating bends that completed a full cycle, meaning that repeated unilateral turning movements were not

included in our frequency analysis. For tail beat number per active bout, unilateral turns were a half cycle (0.5).

In addition to automatically tracking the axial kinematics, we manually estimated sensory input during prey capture at the onset of each bout. Measurements included the distance from the center of the paramecium to the center of the fish's head (r_{prey}), the angle between the long axis of the fish and the center of the prey (θ_{prey}, rightward is negative), and the angle of a paramecium's direction of movement relative to a line between the paramecium and the center of the fish's head (ϕ_{prey}; Fig. 1D). Paramecium velocities were calculated by dividing the distance they moved during the bout by the bout duration. For statistical analysis of paramecium direction of movement, data were transformed such that a value of 90 deg represented a movement directly towards the larvae, while 270 deg was directly away from it. We also evaluated the orientation of the eyes relative to one another (vergence angle) and relative to the prey location, using the long axes of the eyes (Fig. 1D) and the prey. For comparative assessments of vergence in IR-illuminated conditions, we used the time point immediately prior to movement and the point at which the larvae successfully or unsuccessfully consumed the paramecium.

Manual analysis of eye angle and prey position at the onset of each bout was performed using a custom-written MATLAB analysis program (MathWorks, Natick, MA, USA). To avoid any experimenter bias in measurements, we randomly shuffled the order of digitized video frames prior to manual measurements. Data were processed using custom-written MATLAB analysis programs. Statistical analyses were performed using StatPlus Professional (AnalystSoft, Vancouver, BC, Canada) and tests of normality were performed to determine whether parametric *versus* non-parametric examinations were appropriate. Consequently, correlations were determined using either Spearman's rank test (reported as ρ) or Pearson's product-moment test (reported as R). Comparisons of two independent samples were performed using Mann–Whitney U-tests or Student's t-test, while two related samples were compared using either Wilcoxon matched pairs test or a paired two-sample t-test. Where appropriate, degrees of freedom are reported parenthetically with the respective ρ, R or t values, according to convention. Data are reported in the text as means ± s.d.

RESULTS

Capture behavior was initiated with the prey at azimuth angles from 110 to –110 deg with respect to the larvae's midsagittal plane and distances of up to 3 mm (range 0.34–2.99 mm; N=50). Fig. 1E shows an example of a full capture sequence, illustrating the automated measurements of tail curvature, distance traveled by the larva and the change in heading while tracking a paramecium. Larvae initiated a capture maneuver once paramecia were within 0.5 mm of the mouth (mean 0.53±0.19 mm, range 0.27–1.09 mm; N=50). The whole process from detection to consumption took just over a second, on average (mean 1.2±0.6 s, range 0.3–2.7 s; N=50). Prey capture in zebrafish larvae is, by necessity, an iterative process (Fig. 1E), as they fragment their movements into 'bouts' of activity and 'intervals' of inactivity termed 'beat-and-glide' swimming (Buss and Drapeau, 2001; Masino and Fetcho, 2005). We found a positive correlation between the number of active bouts and the proximity of the paramecia (R_{48}=0.30, P<0.05, N=50; range 2–11 bouts). The duration of bouts was around 200 ms (mean 188.7±78.8 ms, range 76–552 ms; N=233), with 2–3 tail beats per bout (mean 2.5±1.6, range 0–10; N=233). The interval between successive bouts was about half the mean duration of a bout (mean 93.3±130.2 ms, range 0–1084 ms; N=183). While the range of bout durations remained relatively constant during prey capture, we found a significant decrease in the interval between bouts related to distance to prey (ρ_{181}=0.44, P<0.001). Collectively, these data suggest that larvae generate more fixed-duration bouts to chase down more distant prey and that the interval between bouts decreases as they get closer. However, our principal interest here was potential differences in kinematics within bouts and how these may relate to prey location. We began by assessing features of the initial orientation turn that may scale with prey azimuth.

Initial turn speed and magnitude scale with prey azimuth

Fig. 2 shows examples of orientation turns to paramecia located at low (Fig. 2A), intermediate (Fig. 2B) and high (Fig. 2C) azimuth angles. A comparison of maximum larval angular velocity *versus* prey azimuth reveals a significant correlation between the two measurements (Fig. 2D), suggesting larvae generate faster turns when prey are detected at higher azimuth. During orientation turns, the maximum amount of tail curvature appeared to be near the caudal end. To confirm this, we examined the rostral-most bend location of the tail and the region of the tail that exhibited the maximum degree of curvature for all turns, as in Fig. 2E,F. While axial bending is more apparent rostrally with increased angular velocity (Fig. 2E), the location of maximum curvature during turns is consistently near the caudal end of the tail (Fig. 2F).

We next examined whether the angle of the initial turn correctly aligned the larva to the perceived location of the paramecium (Fig. 3A). We found a significant correlation between the angle of the initial turn and prey azimuth (R_{48}=0.93, P<0.001, N=50). Surprisingly, however, this response consistently underestimated the azimuth of the prey at the point of detection (Fig. 3B). We found no correlation between prey azimuth and the number of bends in bouts that included only turning maneuvers (R_{31}=0.29, P=0.10, N=33, range 1–4 bends), suggesting that the size of the initial turn accounts for a large proportion of the orientation response. If zebrafish larvae were recognizing the movement of paramecia and generating a predictive turn, then the under-turns may have been a consequence of paramecia consistently moving toward them. However, there were roughly equal numbers of paramecia moving toward (N=22) *versus* away from (N=28) the medial axis of zebrafish larvae, which argues against any predictive turning response.

Movements following initial turns are also biased by prey location

The initial orientation turn helps align larvae appropriately to paramecia, but there are also movements that follow the first tail bend. We next investigated whether these movements were also biased in the direction of prey. If the paramecium was directly in front of the larva, the larva tended to perform symmetrical, forward swimming movements (Fig. 4A), while at higher prey azimuth angles the response was typically one or more unilateral turns (Fig. 4C). If paramecia were detected at lower azimuth angles, an initial bend was followed by asymmetrical swimming that closed the angle to the prey (Fig. 4B). To quantify these observations, we examined the relative asymmetry of time-varying curvature at a fixed location (19% from the tip of the tail, arrows in Fig. 4A–C) for every fish on a bout-by-bout basis. This location was selected because it represented, on average, the site of maximum tail curvature for all bouts of movement (19±12% from the tip of the tail, N=183; see also Fig. 2F). We then compared curvature (κ) for leftward and rightward tail bends and related this to prey azimuth (Fig. 4A′–C′).

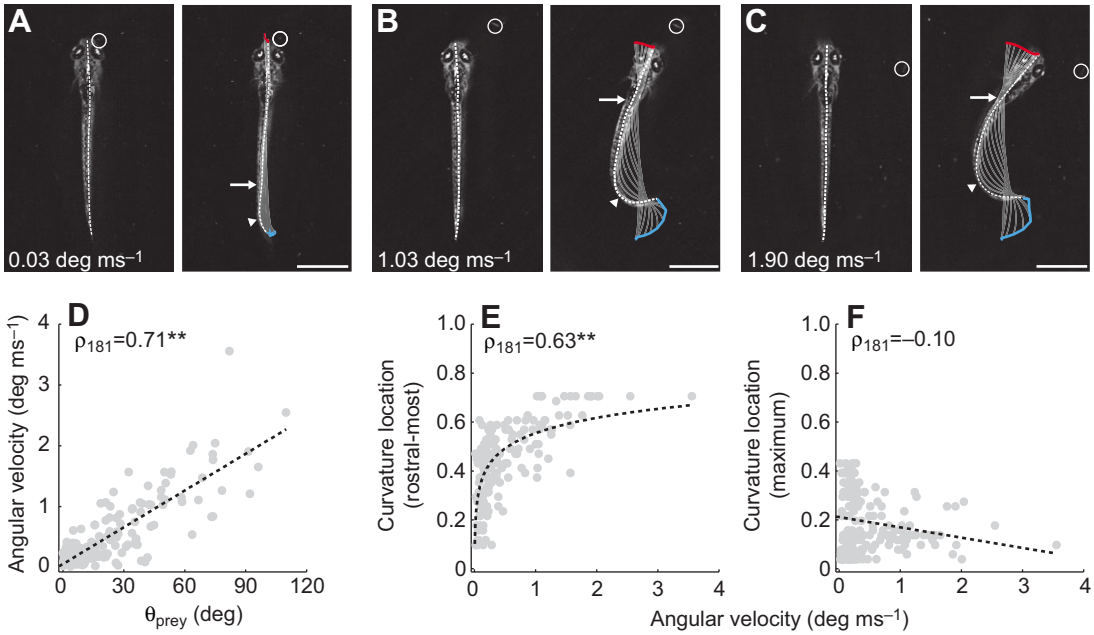

Fig. 2. Speed and shape of the initial turn following prey detection. (A–C) Frames from high-speed videos illustrating differences in the speed of turns related to prey location. Paramecium location varies in azimuth, from small to large angles (A–C) from the mid-sagittal plane. The speed of turns is indicated in the respective panels. The locations of the most rostral and maximum curvatures are indicated with arrows and arrowheads, respectively. Frames on the left are a single snapshot of the larva just prior to movement, while those on the right are the point of maximum curvature during the turn. In this and subsequent figures, gray lines represent the midline of the fish and are presented at 4 ms intervals to demonstrate the change in curvature during this period. Movement of the mouth (red) and the tip of the tail (blue) is also shown. A circle indicates paramecium location. All scale bars, 1 mm. (D) The maximum angular velocity generated during the initial turn scales with the absolute value of the azimuth of the paramecium (θ_{prey}, N=183 bends during 50 capture trials in 17 larvae). Trend line is a linear fit. (E) The most rostral location at which bending was observed above 0.4 mm^{-1} plotted against the magnitude of the angular velocity of turns. Axial bending occurs more rostral with increased angular velocity. Body length is normalized from 0 (tip of the tail) to 1 (tip of the head). We can track this relationship up to the level of the swim bladder (~0.7), beyond which curvature values were set to 0 mm^{-1} (see Materials and methods). Trend line is a linear fit to the natural log of curvature location *versus* angular velocity. (F) The location of maximum tail curvature does not vary systematically with angular velocity. Body length is normalized from 0 (tip of the tail) to 1 (tip of the head). Trend line is a linear fit. **P<0.001 following Spearman's rank test (ρ).

As confirmation of the utility of this measure, we observed significant differences in integrated curvature ($\Sigma\kappa$) that were systematically correlated with prey azimuth (Fig. 4D). To distinguish between turning and swimming movements, we normalized the integral of curvature *versus* time from the beginning to the end of each bout (see Materials and methods, Eqn 3), which allowed us to separate unilateral turning movements to the right or left (values of –1 or 1, respectively) from perfectly symmetrical swimming movements (values nearest 0) and asymmetrical swimming movements (values that fall in between). As shown in Fig. 4E, the normalized data show a clear biasing of leftward and rightward movements according to the angle of the paramecium on the left or right side. Crucially, however, the data are not simply trimodal (e.g. only 0 and ±1); instead, there are values that consistently fall between these extremes, as you would expect for biased swimming movements.

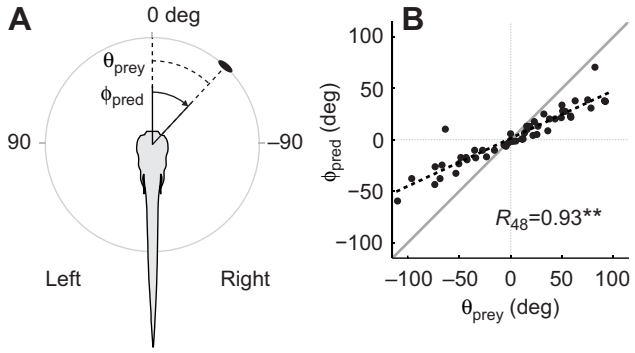

Fig. 3. Magnitude of the initial turn based on prey location. (A) Diagram illustrating the prey azimuth (θ_{prey}, dashed lines) and the corresponding turn angle of the larva (ϕ_{pred}, solid lines). Locations and turns to the right are negative, those to the left are positive. (B) Turn angles (ϕ_{pred}) relative to prey azimuth (θ_{prey}) at the very beginning of the capture behavior. The thick gray line represents unity, where the response would precisely match prey location. Larvae consistently underestimated prey location, as demonstrated by the relatively shallow slope compared with unity. Trend line is a linear fit. **P<0.001 following Pearson's product-moment test (R).

We defined forward movement as longitudinal velocities greater than 0 mm s^{-1} and backward movement as values less than 0 mm s^{-1}. During a prey capture sequence, larvae not only moved forward or to the side but also often moved backward. In comparison to forward movement, backward movement was characterized by higher curvature (2.3±1.2 mm^{-1} for backward, N=55, *versus* 1.4±0.7 mm^{-1} for forward, N=128; U=5003, Z=4.51, P<0.001), more caudally located tail bends (15±9% for backward, N=55, *versus* 21±13% for forward, N=128; t_{181}=3.0, P<0.01) (Fig. 5A,B) and repeated bilateral abduction of the pectoral fins (not shown).

We then examined the context in which backward movements were triggered. When the location of paramecia was plotted according to whether a forward or backward movement of the larvae was evoked, as in Fig. 5C,D, there was a large degree of overlap in paramecium location, eliminating the possibility that backing up is occurring in response to the prey being too close to attack. Because we manually tracked the direction of movement of paramecia in

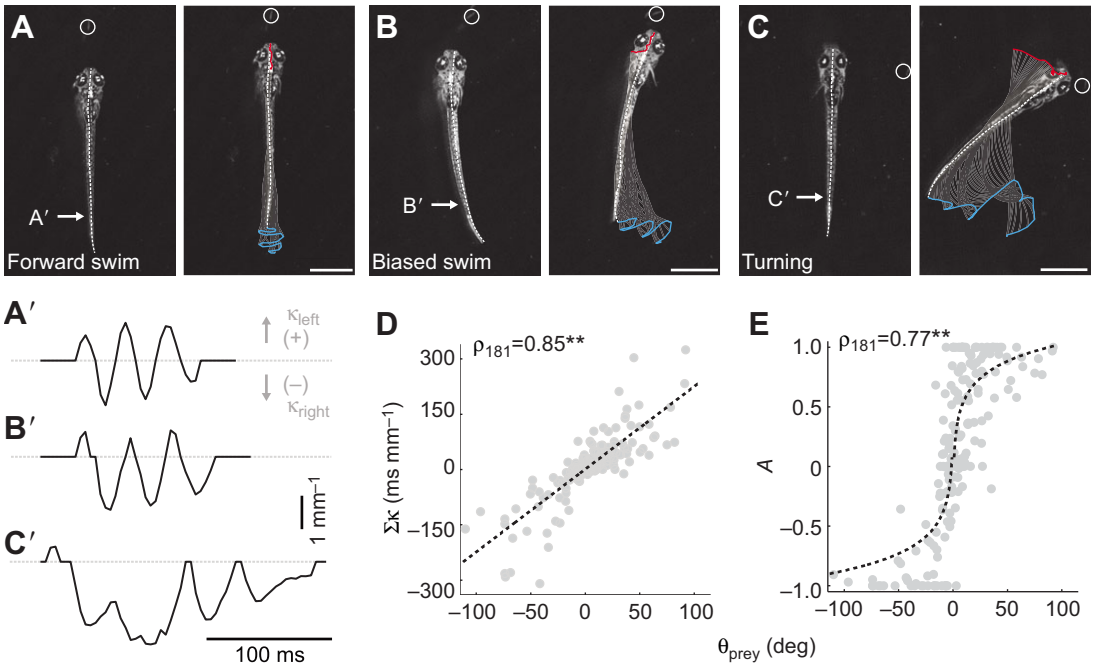

Fig. 4. Biasing of movements following the initial turn. (A–C) Frames from high-speed videos illustrating differences in the directionality of movements following the initial orientation turn. These range from forward swimming (A), to biased swimming (B), to unilateral turning (C). Frames on the left are a single snapshot of the larva just prior to movement, while those on the right are at the completion of the movement. Other conventions are as indicated in Fig. 2A–C. All scale bars, 1 mm. In A′–C′, raw curvature data from the regions indicated by the arrows in A–C provide a means to quantify the relative symmetry of leftward curvature (positive κ values) and rightward curvature (negative κ values) with respect to paramecium location. As paramecium location progressively moves to the right, so too does the weight of curvature to the right side, from symmetrical swimming (A′) to biased swimming (B′) to turning (C′). Dashed gray line indicates zero curvature. (D) Integrated curvature (Σκ) varies systematically with the azimuth of the prey (N=183 bouts). Trend line is a linear fit. (E) A normalized measure of tail movement asymmetry (A, Eqn 3) also varies with paramecium location. A tail movement asymmetry value of 0 represents symmetrical displacement whereas asymmetries of 1 or –1 represent exclusively leftward or rightward displacement, respectively (see Materials and methods). There is saturation of this relationship as asymmetries approach completely leftward or rightward displacements (N=183 bouts). Trend line is a linear fit to the natural log of movement asymmetry *versus* prey azimuth. **P<0.001 following Spearman's rank test (ρ).

addition to the movement of zebrafish larvae, we then asked whether the selection of movement direction was based on whether the paramecium was moving away from or toward the larva.

As larvae tracked their prey, the paramecia moved in all directions (Fig. 5E). Compared with the speed of zebrafish larvae (mean 8.2±6.0 mm s^{-1}, range 1.2–44.6 mm s^{-1}; N=233), paramecia movements were relatively slow (mean 1.1±0.7 mm s^{-1}, range, 0.1–4.1 mm s^{-1}; N=183). We took a conservative approach to analyzing the data and focused on the direction of paramecium movement that evoked the fastest backward and forward movements in larvae leading up to the capture maneuver. Fig. 5F illustrates five different contours in ever increasing 10% increments representing the top 50% of larval velocities for both forward (red) and backward (blue) movements (i.e. 0–10% of the fastest responses is the inner contour while 0–50% is the outer one). From this analysis, a clear pattern emerges. If paramecia were moving away from the larva, a fast forward movement was more likely, while the opposite was true if they were moving toward them. Regardless of whether the top 10% or the top 50% were included for statistical analysis, there were significant differences in larval response based on the direction in which paramecia were moving (see Fig. 5 legend for statistical details).

Selection of ram *versus* suction capture strategies depends on prey location

To consume prey, larval fish use strategies that largely fall into two categories: (1) ram captures, where prey are engulfed following forward movements, or (2) suction captures, where they are engulfed with little or no body movements (Norton and Brainerd, 1993). During the final capture maneuver, we observed both ram-type movements (Fig. 6A) and suction-type movements (Fig. 6B). As the larvae consumed the paramecia, the head snapped upwards coincident with the opening of the mouth (Fig. 6C,D). Because our videos were filmed from above, we could not quantify the degree of dorsal flexion. However in 44 out of 50 capture attempts, dorsal flexion at engulfment was observed, suggesting paramecia were primarily captured from below. While the method of ingestion is relatively consistent, the decision to consume prey using ram *versus* suction strategies appeared to rely on the proximity of the paramecium to the zebrafish.

To evaluate this possibility, we compared the relative distance moved by the larval predator with the distance moved by the prey to provide a RSI score (see Materials and methods, Eqn 4). A RSI score of 1 indicates that the capture movement was entirely a ram-type movement, and a RSI score of –1 means the capture consisted solely of suction-type movements. Plotting paramecium distance as a function of RSI scores revealed a significant correlation (Fig. 6E). A significant correlation was also observed when we plotted paramecium distance against longitudinal acceleration of the final capture swim (Fig. 6F). The maximum tail beat frequency was also significantly higher on average during final capture swims (mean 37.2±5.6, range 25–50 Hz; N=38) compared with bouts of swimming leading up to capture (mean 29.7±4.0 Hz, range 19–42 Hz; N=88), as determined by a Student's t-test (t_{124}=2.0; P<0.001).

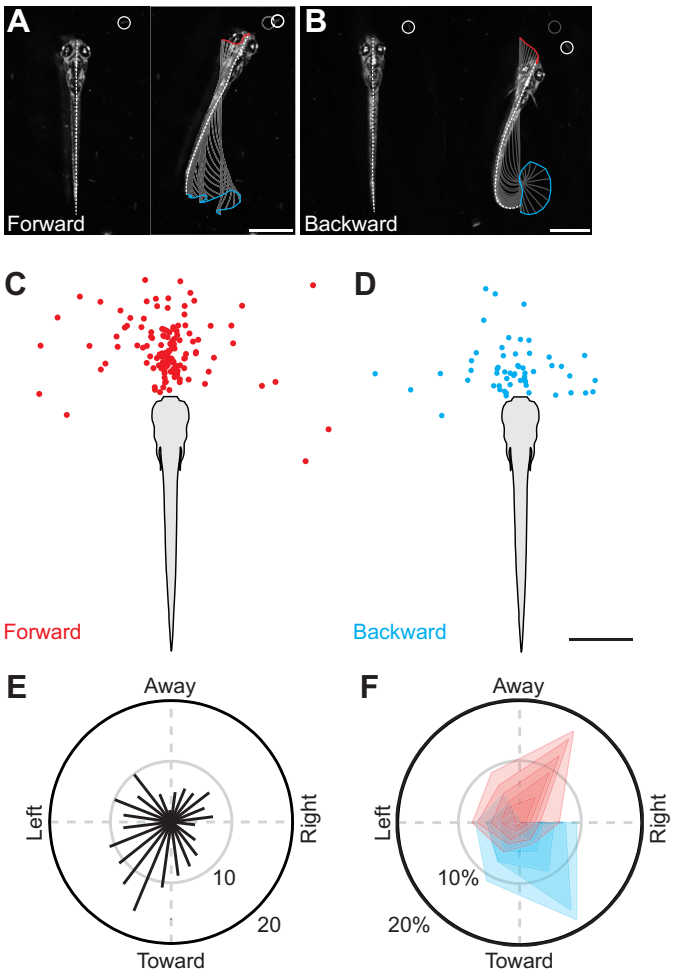

Fig. 5. Forward *versus* backward movement during prey capture. (A,B) Frames from high-speed videos illustrating differences in the direction of larval movement, which appear unrelated to prey location. Based on positive *versus* negative values in longitudinal velocity, movements are described as forward (A) or backward (B). Frames on the left are a single snapshot of the larva just prior to movement, while those on the right track movements up to a fixed time interval (132 ms). Other conventions are as indicated in Fig. 2A–C. All scale bars, 1 mm. (C,D) Location of the paramecium immediately before forward (N=128 bouts, C) or backward (N=55 bouts, D) movements of the larvae. The distributions of paramecia are largely overlapping. Scale bar, 1 mm. (E) Histogram plotted on a polar axis indicating the direction of movement of the paramecia for all trials, relative to the fish. Bar length indicates the number of samples per 15 deg bin (N=183). (F) Polar plot indicating the direction of paramecium movement related to whether the larva moved forward (red) or backward (blue). Contours represent the percentage of the total number of trials per 60 deg bin. From the center outward, each contour represents 10% increments. The first contour is the 90–100th percentile of larval velocity, the second is the 80–100th percentile, and so on to the 50–100th percentile in both the forward (N=128) and backward (N=55) directions. Statistics for the fastest 10–50% of responses using Mann–Whitney U-tests are as follows: 10%: U=11, Z=2.45, P<0.05, N=19; 20%: U=53, Z=2.99, P<0.01, N=37; 30%: U=130, Z=3.52, P<0.001, N=55; 40%: U=258, Z=3.64, P<0.001, N=73; and 50%: U=446, Z=3.81, P<0.001, N=92. Larvae back up when paramecia are moving toward them, but advance when paramecia are moving away.

Assessing the importance of visual input during prey capture behavior

During our observations of tail movements during prey capture, we noticed differences in the positioning of the eyes that appeared to be specific to this behavior. Following the initial detection of paramecia, zebrafish larvae exhibited conjugate inward vergence of the eyes (Fig. 7A). The consequence of eye vergence was an increase in binocular overlap of the proximal visual field. Prior to detecting prey, eye vergence was just above 30 deg on average (mean 32±14 deg, N=50). Immediately before initiation of a capture maneuver (either ram- or suction-type), vergence angle significantly increased to around 70 deg (mean 70±10 deg, t_{49}=2.0, P<0.001, N=50). Immediately following prey capture, vergence angles significantly relaxed from pre-capture values to near pre-detection vergence (mean 44±23 deg, t_{49}=2.0, P<0.001, N=50). We also found that the levels of vergence varied systematically as a function of distance to the prey item, but only after detection (Fig. 7B,C).

To assess what might trigger the decision to capture prey, we first created a two-dimensional (2D) envelope of movement generated by larvae. To do this, we erected a coordinate frame at the body, at the start of each period of activity (bout). Following the end of the bout, we plotted the position of the anterior terminus of the body in that coordinate frame (Fig. 8A). The coordinate frame was placed in a consistent position and orientation with respect to the body across all periods of activity, across all trials. This represents a 2D projection in the coronal plane of the larvae's three-dimensional 'motor volume' (Snyder et al., 2007).

We then created a corresponding 'sensory volume' (Snyder et al., 2007). To do this, we plotted all paramecium locations at detection in the coordinate frame of the closest eye. We next combined the eye-fixed prey detection positions for left and right eyes. Then, we found the locations of prey at the largest temporal and nasal extremes. Finally, a wedge was formed with boundaries at these extremes and an arc length determined by maximum distance of detection across all trials (Fig. 8B). Using the sensory volume, we could estimate whether paramecia would be located within the receptive fields of the temporal *versus* nasal retinas (Fig. 8B). When we used an average of eye vergence prior to detection (32 deg) to create binocular visual fields in body relative coordinates and superimposed this on the location of prey at the point of detection, there was a relatively good match between the union of the two eyes' monocular sensory volumes and prey location in successful capture trials (Fig. 8C). At the point of capture (70 deg vergence, on average), the iterations of axial movements combined with eye vergence placed paramecia in the proximal-most temporal receptive fields of both eyes (Fig. 8D).

Finally, to evaluate the importance of vision in prey capture behavior, we filmed attempts at capturing prey using only IR illumination. In the dark, larvae ignored paramecia at distances that would normally engage an orientation movement (supplementary material Movies 1, 2). However, we did eventually observe 13 failed attempts to consume paramecia and seven successful captures. During dark captures, the movements matched those during proximal captures in lit conditions, namely suction captures involving far caudal tail bends (Fig. 9A). We quantified the location of maximum curvature in successful cases (mean 17±6%; N=7), which was kinematically consistent with caudal tail bends during prey capture movements in the light. We also observed an increase in eye vergence coincident with the capture attempt in 18 out of the 20 trials in the dark (Fig. 9B), from 41±11 to 67±21 deg (Wilcoxon matched pairs test; Z=3.72, P<0.001, N=18). These values match ocular vergence at proximal locations in lit conditions (<1 mm), although vergence in the dark displays a greater degree of variability (Fig. 9C). All of the capture attempts occurred at distances suggesting contact with the mouth and/or head of the larva (Fig. 9D).

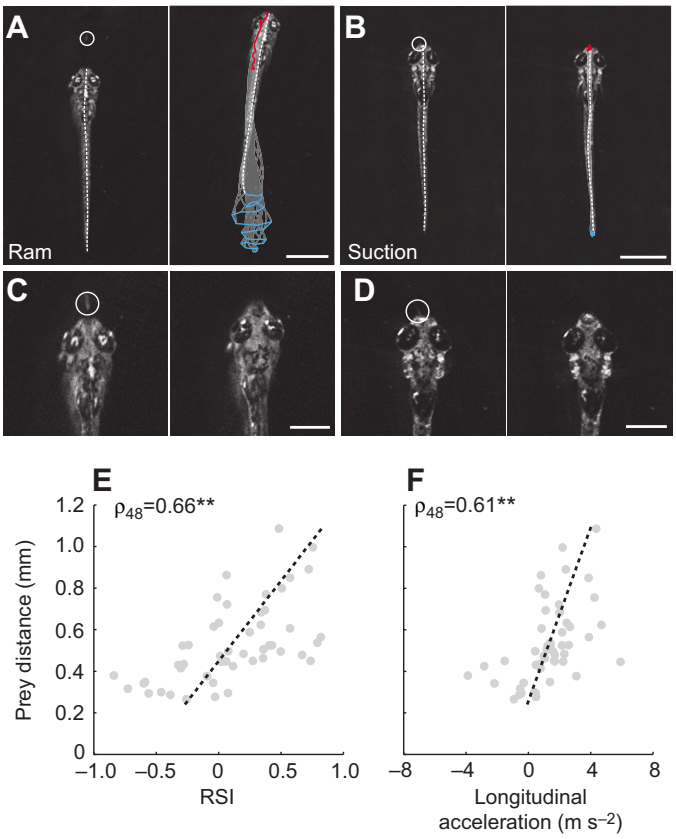

Fig. 6. Different capture strategies based on distance. (A,B) Frames from high-speed videos illustrating the performance of ram-type (A) and suction-type (B) capture maneuvers. Frames on the left are a single snapshot of the larva just prior to movement, while those on the right are at the completion of the movement. Other conventions are as indicated in Fig. 2A–C. Scale bars, 1 mm. (C,D) Higher magnification frames from the same capture sequences as in A and B, illustrating dorsal head flexion during ingestion. Frames on the left are 8 ms before the larvae ingest the paramecia, while frames on the right are at the point of ingestion. A circle indicates paramecium location. Scale bars, 0.5 mm. (E) Distance of the larva from the paramecium *versus* the ram–suction index (RSI) score at the initiation of capture movements demonstrates a gradation in capture response (–1=suction, 1=ram). At short distances, the movements tend to be more suction-like and as distance increases, the movements become more ram-like (N=50). Trend line is a linear fit. (F) Distance of the larva from the paramecium *versus* the maximum longitudinal acceleration of the final capture swim also demonstrates a gradation in response. As the distance from the paramecium increases, the maximum longitudinal acceleration also increases. At the shortest distances, negative accelerations are observed, indicating backward movements (N=50). Trend line is a linear fit. **P<0.001 following Spearman's rank test (ρ).

DISCUSSION

Following prey detection, the goal for a zebrafish larva is to get within striking distance. Our work now provides detailed kinematic information explaining how this is accomplished and what measures are taken to finally consume prey. Our progress was facilitated by a rearing protocol that increased the rate of occurrence of prey captures and by automated analysis that provided an unbiased assessment of axial kinematics. Although previous work has examined the movements generated by larvae during prey capture (Bianco et al., 2011; Borla et al., 2002; McElligott and O'Malley, 2005), this study provides the first demonstration that zebrafish larvae are using visual information to systematically modify their movements from the initial orientation turn to the final capture maneuver.

Circuit mechanisms governing approach

The behavior begins with the detection of prey. Depending on the azimuth of prey at detection, a faster or slower turn is produced. While the first bend accounts for a large portion of the initial orientation to paramecia, it is noteworthy that the initial turn consistently underestimates the actual location of prey regardless of its direction of motion. In adult goldfish, orientation turns exactly match the azimuth of prey (Torres et al., 2005). Comparisons between adult goldfish and larval zebrafish have revealed common neural mechanisms underlying the control of turn intensity (Korn and Faber, 2005), so it is not clear why zebrafish larvae would not also correctly orient to the azimuth of prey. Contributing to the inexplicability of this observation, zebrafish larvae have the ability to process some kinds of prey motion, as demonstrated by backward *versus* forward movements in response to approaching or receding prey (see below). It could be that this discrepancy reflects differences in the saliency of prey looming in, *versus* traversing, the visual field. Regardless, we do see systematic differences in turn speed related to prey azimuth. What neural mechanism might explain this response?

Decades of work have demonstrated the importance of a midbrain region called the optic tectum (or superior colliculus in mammals) in visuomotor integration in a variety of vertebrate species (Angeles Luque et al., 2005; Ingle and Hoff, 1990; Mysore and Knudsen, 2011). As in all vertebrates, the zebrafish tectum is retinotopically organized, meaning visual space is systematically mapped onto neighboring locations in the brain (Baier et al., 1996; Niell and Smith, 2005; Stuermer, 1988). For example, the temporal-most retinal ganglion cells (RGCs) project to the anterior-most tectum. As you move in the nasal direction, RGCs project to progressively more posterior regions of the tectum. Consequently, tectal neurons along the anterior–posterior axis systematically represent anterior–posterior locations in visual space. In zebrafish, retinotectal afferents are largely commissural, so the left tectum processes visual information from the right side, and *vice versa* (Stuermer, 1988). Recently, this anatomical understanding of tectal retinotopy was demonstrated to spectacular effect using *in vivo* functional imaging during the perception of paramecia (Muto et al., 2013).

Given this pattern of organization, it is likely that the location of paramecia in the visual field dictates the magnitude of the initial turn, from slower, smaller turns (temporal retina–anterior tectum) to faster, larger ones (nasal retina–posterior tectum). The existence of a graded axial motor map in the larval zebrafish tectum is consistent with the presence of motor maps in the tectum (or colliculus) in other species, whose function is to generate appropriate orientation movements toward stimuli. For instance, microstimulation of different regions of the tectum/colliculus evoke graded axial movements in lampreys (Saitoh et al., 2007), neck movements in owls (du Lac and Knudsen, 1990), ear movements in cats (Stein and Clamann, 1981) and eye saccades in primates (Robinson, 1972). How might regional differences in tectal activity translate into differences in the firing rates of axial motoneurons?

Neurons in the tectum project to reticulospinal regions in the larval zebrafish (Sato et al., 2007). Turn intensity control *via* reticulospinal neurons in zebrafish larvae has been studied in the context of fast evasive maneuvers, like those generated during escapes. Three segmentally homologous neurons, the Mauthner cell, MiD2cm and MiD3cm, are recruited differentially during stronger *versus* weaker escape bends (Kohashi and Oda, 2008; Liu and Fetcho, 1999;

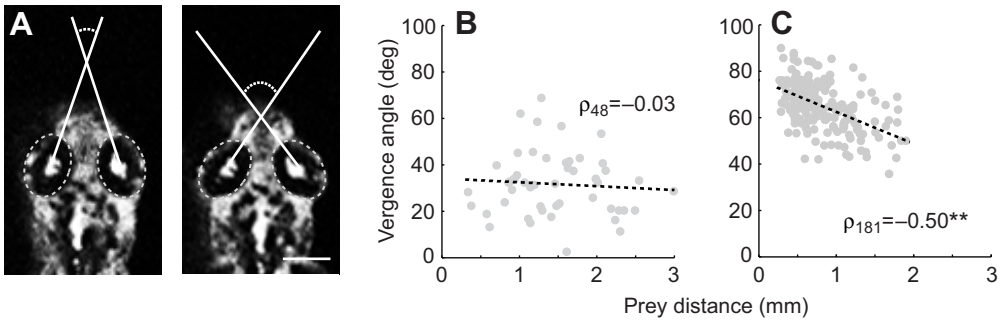

Fig. 7. Conjugate vergence of the eyes during prey capture. (A) Frames from a high-speed video illustrating low (left, 37 deg) and high (right, 71 deg) eye vergence angles. Scale bar, 250 µm. (B) Eye vergence angles immediately before detection of the paramecium (*N*=50). There is no relationship between vergence and distance from prey prior to detection. Trend line is a linear fit. (C) Eye vergence angles immediately after detecting the prey (*N*=183). Vergence data following the capture maneuver are not included here (*N*=50). Once the capture sequence is initiated, the eyes increasingly verge as a function of distance from the paramecium. Trend line is a linear fit. ***P*<0.001 following Spearman's rank test (ρ).

O'Malley et al., 1996). However, studies of premotor excitatory spinal interneurons have revealed that differences in escape bend intensity are graded by changes in the level of firing within the active pool, rather than the recruitment of inactive neurons (Bhatt et al., 2007). Thus, different intensities of bends can be a consequence of engaging different cells or engaging the same ones to different degrees. Therefore, projections from the tectum to reticulospinal neurons could be uniform or selective. Future work examining the projection patterns and functional interactions of tecto-bulbar circuitry in zebrafish should help resolve this issue. But which neurons might they target?

Studies using whole-field motion to generate orientation maneuvers have found segmentally distributed reticulospinal neurons that are selectively active during turns, namely the RoM1r group in rhombomere 1 and ventromedial cells in rhombomeres 3–5 (Orger et al., 2008). Assuming that visual inputs to the tectum are principally commissural, then the command to the spinal cord that generates turns to the same side as the stimulus must cross back over at some point. The RoM1r and ventromedial neurons appear to project ipsilaterally (Kimmel et al., 1982; Metcalfe et al., 1986), so it could be that tectal neurons mediating prey orientation behavior are commissural or that the ipsilateral reticulospinal neurons project to commissural interneurons in the spinal cord, or both. Experiments in cats have revealed a 'double-crossed' pathway, where neurons in the primary motor cortex shape motoneuron activity on the same side *via* contralateral reticulospinal neurons that in turn target commissural spinal neurons (Jankowska et al., 2006). If commissural spinal neurons are involved, then likely candidates derive from the vertebrate p0 progenitor domain (Goulding, 2009), known as V0-eD (excitatory descending) cells in zebrafish (Satou et al., 2012).

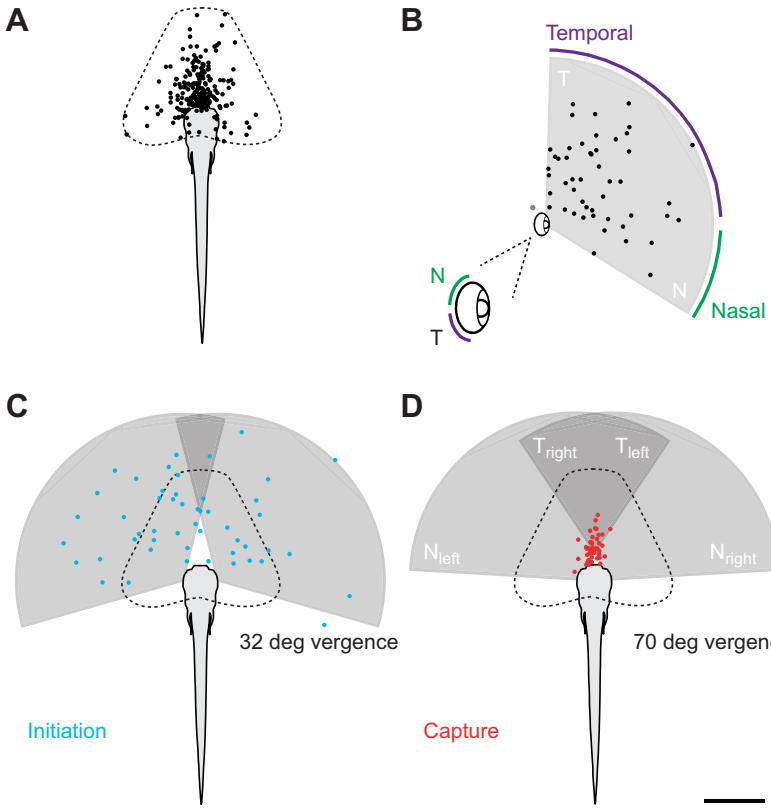

Fig. 8. Motor and sensory volumes during prey capture. (A) Schematic diagram representing the two-dimensional (2D) coronal plane projection of the motor volume of zebrafish larvae during prey capture. This was calculated by plotting the end-point of the mouth for every bout of movement during the 50 prey capture trials (*N*=233) and symmetrically circumscribing the area encompassed by these points. (B) Schematic diagram representing the 2D coronal plane projection of the sensory volume of zebrafish larvae during prey capture. This was calculated by plotting the location of paramecium relative to eye-fixed coordinates immediately prior to the initiation of prey capture behavior (*N*=50). Detection using the left and right eye is represented as a single eye. A cone encompassing paramecia at the furthest distance and largest angles in azimuth was then drawn. A single gray data point outside the field represents a paramecium that came into contact with the larvae and was excluded from our estimation of the sensory volume. The inset is a larger representation of the eye marking the temporal (T) and nasal (N) retina, and the corresponding locations in space representing their receptive fields. (C) Using an average vergence angle just prior to detection (mean 32±14 deg, range 3–69 deg; *N*=50) we can plot the motor volume and monocular sensory volumes and relate this to the location of paramecia at the initiation of prey capture behavior. Paramecia are distributed throughout the union of the two monocular sensory volumes. (D) As in C, we can use an average vergence angle just prior to capture (mean 70±10 deg, range 42–90 deg; *N*=50) and relate both motor and sensory volumes to paramecium location. The culmination of axial and ocular movements places paramecia in a clear 'capture zone' well within the motor volume and the binocular temporal retinal fields. Temporal and nasal receptive fields are indicated for both the right and left eyes. Scale bar, 1 mm.

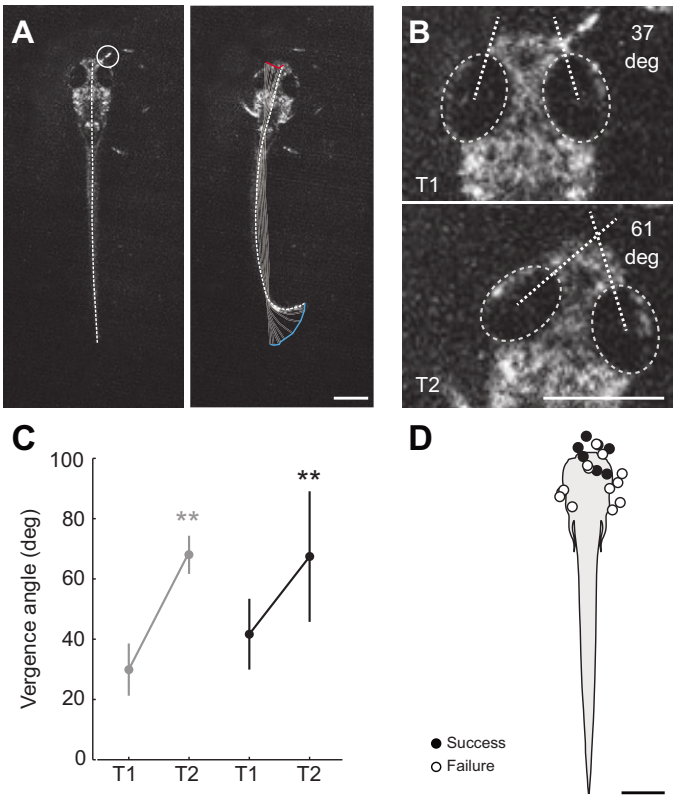

Fig. 9. Prey capture behavior in the dark. (A) Frames from a high-speed video of prey capture behavior in the dark. The frame on the left is a single snapshot of the larva just prior to movement, while that on the right is at the point of capture. Other conventions are as indicated in Fig. 2A–C. Capture movements produced in the dark are very similar to those initiated at close proximity in lit conditions. (B) Images extracted from the prey capture video in A, demonstrating an increase in eye vergence coincident with the suction-like capture strategy. T1, 44 ms before a movement to capture the paramecium; T2, during ingestion. (C) Vergence values at close proximity (<1 mm) in the light immediately before detection (T1) and immediately before capture (T2) are in gray. Vergence values in the dark just before moving to capture the paramecium (T1) and at the point of ingestion (T2) are in black. The significant increase in vergence observed in the dark is similar to that observed at close proximity in the light, albeit more variable. $^{**}P<0.001$, Wilcoxon matched pairs test. (D) Schematic diagram of the locations of paramecia at the initiation of successful dark captures ($N=7$) and unsuccessful attempts ($N=13$). Capture attempts were very rare in the dark and were only initiated when the paramecium was in very close proximity to the fish. All scale bars, 0.5 mm.

Within this population are previously identified multipolar (MCoD) and unipolar (UCoD) commissural descending cells (Hale et al., 2001).

In implicating these cells during orientation turns, the shape the tail adopts is informative. Zebrafish turns are historically named based on the shape of the tail. In both slow and fast orientations to prey described here, the maximum curvature is located nearest the tail, which more closely resembles variations of 'J-bends' (McElligott and O'Malley, 2005) than it does other identified turning responses to sensory stimuli, like 'O-bends' and 'C-starts' (Budick and O'Malley, 2000; Burgess and Granato, 2007; Liu et al., 2012). The zebrafish spinal cord is organized somatotopically, with each body segment innervated by a local pool of axial motoneurons (Myers, 1985). MCoDs have extensive ramifications near the caudal end of the tail where they directly contact motoneurons (McLean et al., 2008). A J-shaped bend is consistent with the activation of commissural spinal neurons with extensive output to caudal motoneurons, especially as many reticulospinal neurons do not project the full length of the spinal cord (Gahtan and O'Malley, 2003). Thus, differences in the speed of the J-bend could be due to a dedicated tecto-reticulo-spinal turning circuit that affects spinal motoneuron firing rate *via* the differential activation of identified spinal commissural interneurons.

After the execution of the first J-bend, larvae continue to orient themselves by biasing the directionality of subsequent actions, which include asymmetric swimming and backward movements. Undulatory swimming is generated by circuits in the spinal cord (Grillner, 2003; Roberts et al., 1998). Much of the focus on so-called spinal central pattern generators (CPGs) has been on patterns of activity that would produce constant forward movements, although symmetrical activity can be altered by reticulospinal drive to control pitch, roll and yaw (Deliagina et al., 2002). Visual stimuli provided by paramecia can evoke forward swimming, suggesting that tectal circuits can activate the spinal CPG. The simplest scenario is that biased swimming is a consequence of convergence between tecto-motor circuits involved in forward CPG activation and those involved in pure turns. Where might this occur?

Tail-beat frequency provides some clues to the potential site of convergence, which again implicates the V0-eD neurons. MCoD cells participate in rhythmic swimming, but only at the frequencies we observed leading up to the capture maneuver (~20–50 Hz), above which they are silent (McLean et al., 2008). Therefore, it is likely that they contribute to motor output during prey capture behavior. However, MCoDs are not anatomically homogeneous. Although many have axon collaterals that ramify caudally, more rostrally located MCoDs also have local axon collaterals that could drive rostral motoneuron activity (McLean et al., 2008). One potential scenario is that more rostral MCoDs alter the shape of the rostral portion of the body, which, if superimposed on symmetrical tail beats driven by more caudal MCoDs, will ultimately bias swimming direction. Like more rostral MCoDs, UCoDs also have local axon collaterals (Satou et al., 2012). However, nothing is known about the activity patterns of UCoDs or their likely connections. It will be interesting to see whether there are differences in the relative participation of MCoD/UCoD neurons during turns or forward *versus* biased swimming related to their rostro-caudal location in spinal cord.

In addition to asymmetric swimming, zebrafish larvae produced backward movements following the detection of prey. Backward movements have been described, but their purpose was unclear (Borla et al., 2002; Zhu et al., 2009). Here we have demonstrated that backward movements are initiated when the larvae are tracking approaching prey. The movements are characterized by high amplitude J-bends and bilateral pectoral fin extension that result in negative longitudinal velocities, which presumably place larvae in a better position to capture prey. The sharpness of the bend (see Fig. 5B) appears sufficient to not only obtain yaw torque for turning but to also cause some fluid to be accelerated toward the head, potentially mediating the majority of the backward thrust. A recent study has identified a region in the anterior–ventral optic tectum that, when activated, generates backward J-bends, pectoral fin abduction and eye vergence (Fajardo et al., 2013). This location is consistent with a region of tectum that might be involved in executing more subtle locomotor maneuvers and a better ability to process complex visual cues (see below).

Our observations suggest that to get within striking distance, larval fish are capable of systematically adjusting their lateral, forward and backward movements based on visual information. The first

report of zebrafish prey capture that coined the term J-bend suggested that it was a relatively stereotyped movement whose repetition (multiple J-bends, called 'J-turns'), interspersed with forward swimming bouts, explained how larvae chase down prey (McElligott and O'Malley, 2005). In light of our findings, this view warrants re-consideration. J-bends are not stereotyped. Their speed and magnitude depend on the azimuth of prey at detection. Also, swimming movements are not strictly forward, but can be biased to the left or right and even backward by the perceived location of the prey and the prey's direction of travel. The commands to do so are most likely conveyed by a commissural motor pathway, for which we posit spinal V0-eD involvement. Given the shared molecular mechanisms regulating spinal cord differentiation in all vertebrates and the corticospinal study in cats discussed above, the targeting of V0 spinal commissural interneurons by ipsilateral reticulospinal drive could be a relatively conserved mechanism for shaping volitional actions.

Circuit mechanisms governing capture

After the axial orientation and approach maneuvers, the behavior ends with the consumption of the paramecium. Consistent with previous reports (Bianco et al., 2011; McElligott and O'Malley, 2005), we found that effective striking distance for larvae at this age is about 0.5 mm, on average. We also found that immediately prior to capture, the eyes were verged inward (Bianco et al., 2011). What was not clear from previous work was whether there is a systematic increase in vergence related to the proximity of prey, which we now demonstrate. Thus, concerted actions of axial and ocular networks ultimately place prey in a proximal binocular 'capture zone'. This combination of events is what most likely leads to the signal that triggers the decision to consume prey. What might this signal be?

Studies of zebrafish retina have identified a ventro-temporal region possessing the highest acuity (Schmitt and Dowling, 1999), analogous to the fovea in primates (La Vail et al., 1991) or the area centralis in felines (Robinson, 1987). Based on our estimates of sensory input and the observation that larvae strike from below, it is very likely that this region is the location on the retina that paramecia fall upon following the vergence of the eyes. However, bilateral activation of this region alone is presumably not sufficient, as there is the possibility of binocular overlap at distances that do not initiate a capture maneuver (see Fig. 8C). Given the progressive vergence of the eyes, one possibility is that an efference copy signal reflecting oculomotor activity provides information about prey proximity (Mays and Gamlin, 1995). In this case, bilateral activation of the ventro-temporal retina combined with an internal readout of a high vergence angle could be synthesized to allow zebrafish to confirm that the target is within striking distance (or within their motor volume as defined here).

From this point the decision to consume the prey with or without axial movements (suction *versus* ram) may be accomplished by processing in the left and right tecta. Ram- and suction-type captures have been observed in zebrafish larvae (Borla et al., 2002; Budick and O'Malley, 2000). What we show is that the longitudinal acceleration and relative contribution of ram *versus* suction to prey capture varies systematically with prey distance. This suggests a pre-calculated gradation in behavior based on the perceived distance of the prey item. There are certainly computational mechanisms that could accomplish this, such as the direction, orientation and size selectivity of tectal neurons (Del Bene et al., 2010; Gabriel et al., 2012; Grama and Engert, 2012; Niell and Smith, 2005; Nikolaou et al., 2012). How these mechanisms help calculate distance or direction of travel of paramecia is unknown. However, the recent demonstration that prey capture movements can be evoked in restrained larvae using visual stimuli that simulate paramecia should facilitate future investigations (Bianco et al., 2011).

The movements that larvae perform to accomplish consumption of prey are very similar to those during the orientation and approach phase, and have been characterized in detail previously (Borla et al., 2002). In the case of ram capture swims, tail-beat frequency is higher on average, up to 50–55 Hz, compared with the 40 Hz maximum frequency observed during swimming in the absence of prey (Budick and O'Malley, 2000). There are differences in the participation of spinal interneuronal networks during different swimming speeds (McLean et al., 2008). Fast (or 'burst') swimming movements rely on a particular set of interneurons, while slower (or 'routine') ones rely on a different set, which include the MCoDs. The recruitment order in the spinal cord is topographically organized, with slower excitatory circuits located ventrally, while faster ones are more dorsal (McLean et al., 2007). While fast movements tend to create a large degree of head yaw, slower ones do not (Müller and van Leeuwen, 2004). As lateral displacement of the head would interfere with visual tracking, it is noteworthy that during prey capture the head remains relatively still.

In our study, tail-beat frequencies are within the range that MCoDs are rhythmically engaged and head yaw is minimal (McLean et al., 2008; Müller and van Leeuwen, 2004). A previous study reported much higher frequency values (>80 Hz), which would appear to conflict with this idea (Borla et al., 2002). It should be noted that their measurements of frequency were derived from 'instantaneous tail beat frequencies', where unilateral bend intervals were doubled to estimate frequency. As we measured true tail beat frequencies, we are confident that the spinal networks likely to be responsible for swimming during prey capture are those that normally control rhythmic swimming during routine swimming behavior, albeit at their fastest operational limits.

Importance of vision during prey capture

The entire process leading up to capture, from the detection of prey at further distances and the concomitant execution of graded motor responses, relies on visual input. Previous work examining the importance of vision for capturing prey has assessed the number of surviving paramecia in lit *versus* dark conditions (Gahtan et al., 2005; McElligott and O'Malley, 2005; Smear et al., 2007). These studies demonstrate that more paramecia survive when larvae are deprived of visual input. However, paramecia numbers do decline, suggesting that larvae can consume them in the dark. Until now, the method larvae used to capture prey in the absence of vision was unknown. We found, perhaps unsurprisingly, that dark capture attempts by larvae were performed at locations consistent with paramecia directly contacting their anterior extremities. What was surprising, however, was that larvae produced movements bearing striking similarity to proximal movements in lit conditions, namely J-bends and eye vergence. The execution of prey capture movements was thought to exclusively rely on visual input (McElligott and O'Malley, 2005). The most likely explanation is that larvae rely on somatosensory (e.g. tactile or lateral line) cues to capture prey in the dark. If this is the case, then these sensory modalities also activate the ocular and axial networks engaged during prey capture maneuvers. How might this be achieved?

The tectum (or colliculus) is a major site of sensorimotor integration beyond just visual processing. In a variety of species there are topographic representations of sensations that also register appropriately with tectal motor maps. These include electroreception

in weakly electric fishes (Bastian, 1982), thermosensation in rattlesnakes (Hartline et al., 1978), echolocation in bats (Valentine and Moss, 1997), audition in barn owls (Knudsen, 1982) and somatosensation in cats (Stein et al., 1976). While less is known about other sensory inputs to the zebrafish tectum, given the conserved nature of tectal organization it is likely a similar co-registration of different sensory modalities exists. This could explain why paramecia contacting the larvae evoked ocular and axial movements indistinguishable from proximal visual stimuli. Alternatively, somatosensory modalities may directly access the reticulospinal populations themselves. Ablation experiments have demonstrated the importance of the optic tectum in visually guided prey capture (Del Bene et al., 2010; Gahtan et al., 2005). It will be interesting to see how cutaneous or lateral line inputs may map onto the tectum and whether their contribution to prey capture is also disrupted by tectal ablations.

CONCLUSIONS

Our findings suggest that larvae exert graded control of their ocular and axial musculature to detect, approach and consume prey. The kinematics provided here and the history of zebrafish neurobiology research enabled predictions about the nature of information flow from retina to tectum to brainstem to spinal cord. The task now is to test them. Before doing so, it is worth considering the role of development. The high acuity ventro-temporal region of the retina in 5–7 day old larvae is the last to differentiate (Schmitt and Dowling, 1999), as are the networks in the brainstem and spinal cord responsible for the slower locomotor maneuvers used during prey capture (Kimura et al., 2006; Kinkhabwala et al., 2011; Koyama et al., 2011; McLean et al., 2007; Satou et al., 2012). The sequential emergence of reticulospinal and spinal populations generates a topographic arrangement of cell bodies and their respective dendrites/axons in the neuropil. Therefore, the existence of a developmental ‘chronotopic’ map could explain the orderly assembly of functional interactions between spatially distributed sensory and motor networks. Such a pattern could simplify the pursuit of principles underlying visually guided behaviors using this highly accessible model system.

ACKNOWLEDGEMENTS

We are extremely grateful to Ethan Coffel for his help adapting the fish-tracking program, to Alexandra Salomon for her help with preliminary dark capture data analysis, to members of the MacIver and McLean labs for feedback and comments on the manuscript, and to Matthew Chiarelli for his expert fish care.

AUTHOR CONTRIBUTIONS

B.W.P., M.A.M. and D.L.M. conceived and designed the experiments and wrote the article. B.W.P. performed the experiments and analysed the data. A.O.A. digitized and helped analyse the video data.

COMPETING INTERESTS

No competing interests declared.

FUNDING

This work was supported by the National Science Foundation’s Integrative Graduate Education and Research Training program [DGE-0903637]; a National Science Foundation grant [IOS-0846032 to M.A.M.]; a National Institutes of Neurological Disorders and Stroke grant [R01-NS067299 to D.L.M.]; and fellowships from The Esther A. and Joseph Klingenstein Fund, The Searle Scholars Program, and The Alfred P. Sloan Foundation to D.L.M. Deposited in PMC for release after 12 months.

REFERENCES

Ahrens, M. B., Li, J. M., Orger, M. B., Robson, D. N., Schier, A. F., Engert, F. and Portugues, R. (2012). Brain-wide neuronal dynamics during motor adaptation in zebrafish. *Nature* **485**, 471-477.

Angeles Luque, M., Pilar Pérez-Pérez, M., Herrero, L. and Torres, B. (2005). Involvement of the optic tectum and mesencephalic reticular formation in the generation of saccadic eye movements in goldfish. *Brain Res. Brain Res. Rev.* **49**, 388-397.

Baier, H., Klostermann, S., Trowe, T., Karlstrom, R. O., Nüsslein-Volhard, C. and Bonhoeffer, F. (1996). Genetic dissection of the retinotectal projection. *Development* **123**, 415-425.

Bastian, J. (1982). Vision and electroreception - integration of sensory information in the optic tectum of the weakly electric fish *Apteronotus albifrons*. *J. Comp. Physiol.* **147**, 287-297.

Bhatt, D. H., McLean, D. L., Hale, M. E. and Fetcho, J. R. (2007). Grading movement strength by changes in firing intensity versus recruitment of spinal interneurons. *Neuron* **53**, 91-102.

Bianco, I. H., Kampff, A. R. and Engert, F. (2011). Prey capture behavior evoked by simple visual stimuli in larval zebrafish. *Front Syst. Neurosci.* **5**, 101.

Borla, M. A., Palecek, B., Budick, S. and O’Malley, D. M. (2002). Prey capture by larval zebrafish: evidence for fine axial motor control. *Brain Behav. Evol.* **60**, 207-229.

Borst, A. (2009). *Drosophila*’s view on insect vision. *Curr. Biol.* **19**, R36-R47.

Brownstone, R. M. and Stuart, D. G. (2011). Whither motoneurons? *Brain Res.* **1409**, 93-103.

Budick, S. A. and O’Malley, D. M. (2000). Locomotor repertoire of the larval zebrafish: swimming, turning and prey capture. *J. Exp. Biol.* **203**, 2565-2579.

Burgess, H. A. and Granato, M. (2007). Modulation of locomotor activity in larval zebrafish during light adaptation. *J. Exp. Biol.* **210**, 2526-2539.

Buss, R. R. and Drapeau, P. (2001). Synaptic drive to motoneurons during fictive swimming in the developing zebrafish. *J. Neurophysiol.* **86**, 197-210.

Del Bene, F., Wyart, C., Robles, E., Tran, A., Looger, L., Scott, E. K., Isacoff, E. Y. and Baier, H. (2010). Filtering of visual information in the tectum by an identified neural circuit. *Science* **330**, 669-673.

Deliagina, T. G., Zelenin, P. V. and Orlovsky, G. N. (2002). Encoding and decoding of reticulospinal commands. *Brain Res. Brain Res. Rev.* **40**, 166-177.

du Lac, S. and Knudsen, E. I. (1990). Neural maps of head movement vector and speed in the optic tectum of the barn owl. *J. Neurophysiol.* **63**, 131-146.

Fajardo, O., Zhu, P. and Friedrich, R. W. (2013). Control of a specific motor program by a small brain area in zebrafish. *Front. Neural Circuits* **7**, 67.

Fontaine, E., Lentink, D., Kranenbarg, S., Müller, U. K., van Leeuwen, J. L., Barr, A. H. and Burdick, J. W. (2008). Automated visual tracking for studying the ontogeny of zebrafish swimming. *J. Exp. Biol.* **211**, 1305-1316.

Gabriel, J. P., Trivedi, C. A., Maurer, C. M., Ryu, S. and Bollmann, J. H. (2012). Layer-specific targeting of direction-selective neurons in the zebrafish optic tectum. *Neuron* **76**, 1147-1160.

Gahtan, E. and O’Malley, D. M. (2003). Visually guided injection of identified reticulospinal neurons in zebrafish: a survey of spinal arborization patterns. *J. Comp. Neurol.* **459**, 186-200.

Gahtan, E., Tanger, P. and Baier, H. (2005). Visual prey capture in larval zebrafish is controlled by identified reticulospinal neurons downstream of the tectum. *J. Neurosci.* **25**, 9294-9303.

Goulding, M. (2009). Circuits controlling vertebrate locomotion: moving in a new direction. *Nat. Rev. Neurosci.* **10**, 507-518.

Grama, A. and Engert, F. (2012). Direction selectivity in the larval zebrafish tectum is mediated by asymmetric inhibition. *Front. Neural Circuits* **6**, 59.

Green, M. H., Ho, R. K. and Hale, M. E. (2011). Movement and function of the pectoral fins of the larval zebrafish (*Danio rerio*) during slow swimming. *J. Exp. Biol.* **214**, 3111-3123.

Grillner, S. (2003). The motor infrastructure: from ion channels to neuronal networks. *Nat. Rev. Neurosci.* **4**, 573-586.

Guibé, M., Boal, J. G. and Dickel, L. (2010). Early exposure to odors changes later visual prey preferences in cuttlefish. *Dev. Psychobiol.* **52**, 833-837.

Hale, M. E., Ritter, D. A. and Fetcho, J. R. (2001). A confocal study of spinal interneurons in living larval zebrafish. *J. Comp. Neurol.* **437**, 1-16.

Hartline, P. H., Kass, L. and Loop, M. S. (1978). Merging of modalities in the optic tectum: infrared and visual integration in rattlesnakes. *Science* **199**, 1225-1229.

Ingle, D. J. and Hoff, K. V. (1990). Visually elicited evasive behavior in frogs. *Bioscience* **40**, 284-291.

Jankowska, E., Stecina, K., Cabaj, A., Pettersson, L. G. and Edgley, S. A. (2006). Neuronal relays in double crossed pathways between feline motor cortex and ipsilateral hindlimb motoneurones. *J. Physiol.* **575**, 527-541.

Jessell, T. M., Sürmeli, G. and Kelly, J. S. (2011). Motor neurons and the sense of place. *Neuron* **72**, 419-424.

Kimmel, C. B., Powell, S. L. and Metcalfe, W. K. (1982). Brain neurons which project to the spinal cord in young larvae of the zebrafish. *J. Comp. Neurol.* **205**, 112-127.

Kimura, Y., Okamura, Y. and Higashijima, S. (2006). alx, a zebrafish homolog of Chx10, marks ipsilateral descending excitatory interneurons that participate in the regulation of spinal locomotor circuits. *J. Neurosci.* **26**, 5684-5697.

Kinkhabwala, A., Riley, M., Koyama, M., Monen, J., Satou, C., Kimura, Y., Higashijima, S. and Fetcho, J. (2011). A structural and functional ground plan for neurons in the hindbrain of zebrafish. *Proc. Natl. Acad. Sci. USA* **108**, 1164-1169.

Knudsen, E. I. (1982). Auditory and visual maps of space in the optic tectum of the owl. *J. Neurosci.* **2**, 1177-1194.

Kohashi, T. and Oda, Y. (2008). Initiation of Mauthner- or non-Mauthner-mediated fast escape evoked by different modes of sensory input. *J. Neurosci.* **28**, 10641-10653.

Korn, H. and Faber, D. S. (2005). The Mauthner cell half a century later: a neurobiological model for decision-making? *Neuron* **47**, 13-28.

Koyama, M., Kinkhabwala, A., Satou, C., Higashijima, S. and Fetcho, J. (2011). Mapping a sensory-motor network onto a structural and functional ground plan in the hindbrain. *Proc. Natl. Acad. Sci. USA* **108**, 1170-1175.

La Vail, M. M., Rapaport, D. H. and Rakic, P. (1991). Cytogenesis in the monkey retina. *J. Comp. Neurol.* **309**, 86-114.

Landgraf, M. and Thor, S. (2006). Development and structure of motoneurons. *Int. Rev. Neurobiol.* **75**, 33-53.
Liu, K. S. and Fetcho, J. R. (1999). Laser ablations reveal functional relationships of segmental hindbrain neurons in zebrafish. *Neuron* **23**, 325-335.
Liu, Y. C., Bailey, I. and Hale, M. E. (2012). Alternative startle motor patterns and behaviors in the larval zebrafish (*Danio rerio*). *J. Comp. Physiol. A* **198**, 11-24.
Masino, M. A. and Fetcho, J. R. (2005). Fictive swimming motor patterns in wild type and mutant larval zebrafish. *J. Neurophysiol.* **93**, 3177-3188.
Masland, R. H. (2012). The neuronal organization of the retina. *Neuron* **76**, 266-280.
Mays, L. E. and Gamlin, P. D. (1995). Neuronal circuitry controlling the near response. *Curr. Opin. Neurobiol.* **5**, 763-768.
McElligott, M. B. and O'Malley, D. M. (2005). Prey tracking by larval zebrafish: axial kinematics and visual control. *Brain Behav. Evol.* **66**, 177-196.
McLean, D. L. and Fetcho, J. R. (2008). Using imaging and genetics in zebrafish to study developing spinal circuits in vivo. *Dev. Neurobiol.* **68**, 817-834.
McLean, D. L., Fan, J., Higashijima, S., Hale, M. E. and Fetcho, J. R. (2007). A topographic map of recruitment in spinal cord. *Nature* **446**, 71-75.
McLean, D. L., Masino, M. A., Koh, I. Y., Lindquist, W. B. and Fetcho, J. R. (2008). Continuous shifts in the active set of spinal interneurons during changes in locomotor speed. *Nat. Neurosci.* **11**, 1419-1429.
Metcalfe, W. K., Mendelson, B. and Kimmel, C. B. (1986). Segmental homologies among reticulospinal neurons in the hindbrain of the zebrafish larva. *J. Comp. Neurol.* **251**, 147-159.
Müller, U. K. and van Leeuwen, J. L. (2004). Swimming of larval zebrafish: ontogeny of body waves and implications for locomotory development. *J. Exp. Biol.* **207**, 853-868.
Muto, A., Ohkura, M., Abe, G., Nakai, J. and Kawakami, K. (2013). Real-time visualization of neuronal activity during perception. *Curr. Biol.* **23**, 307-311.
Myers, P. Z. (1985). Spinal motoneurons of the larval zebrafish. *J. Comp. Neurol.* **236**, 555-561.
Mysore, S. P. and Knudsen, E. I. (2011). The role of a midbrain network in competitive stimulus selection. *Curr. Opin. Neurobiol.* **21**, 653-660.
Nawrocki, L., BreMiller, R., Streisinger, G. and Kaplan, M. (1985). Larval and adult visual pigments of the zebrafish, *Brachydanio rerio*. *Vision Res.* **25**, 1569-1576.
Niell, C. M. and Smith, S. J. (2005). Functional imaging reveals rapid development of visual response properties in the zebrafish tectum. *Neuron* **45**, 941-951.
Nikolaou, N. and Meyer, M. P. (2012). Imaging circuit formation in zebrafish. *Dev. Neurobiol.* **72**, 346-357.
Nikolaou, N., Lowe, A. S., Walker, A. S., Abbas, F., Hunter, P. R., Thompson, I. D. and Meyer, M. P. (2012). Parametric functional maps of visual inputs to the tectum. *Neuron* **76**, 317-324.
Norton, S. F. and Brainerd, E. L. (1993). Convergence in the feeding mechanics of ecomorphologically similar species in the centrarchidae and cichlidae. *J. Exp. Biol.* **176**, 11-29.
O'Malley, D. M., Kao, Y. H. and Fetcho, J. R. (1996). Imaging the functional organization of zebrafish hindbrain segments during escape behaviors. *Neuron* **17**, 1145-1155.
Orger, M. B., Kampff, A. R., Severi, K. E., Bollmann, J. H. and Engert, F. (2008). Control of visually guided behavior by distinct populations of spinal projection neurons. *Nat. Neurosci.* **11**, 327-333.
Roberts, A., Soffe, S. R., Wolf, E. S., Yoshida, M. and Zhao, F. Y. (1998). Central circuits controlling locomotion in young frog tadpoles. *Ann. N. Y. Acad. Sci.* **860**, 19-34.
Robinson, D. A. (1972). Eye movements evoked by collicular stimulation in the alert monkey. *Vision Res.* **12**, 1795-1808.
Robinson, S. R. (1987). Ontogeny of the area centralis in the cat. *J. Comp. Neurol.* **255**, 50-67.
Saitoh, K., Ménard, A. and Grillner, S. (2007). Tectal control of locomotion, steering, and eye movements in lamprey. *J. Neurophysiol.* **97**, 3093-3108.
Sanes, J. R. and Zipursky, S. L. (2010). Design principles of insect and vertebrate visual systems. *Neuron* **66**, 15-36.
Sato, T., Hamaoka, T., Aizawa, H., Hosoya, T. and Okamoto, H. (2007). Genetic single-cell mosaic analysis implicates ephrinB2 reverse signaling in projections from the posterior tectum to the hindbrain in zebrafish. *J. Neurosci.* **27**, 5271-5279.
Satou, C., Kimura, Y. and Higashijima, S. (2012). Generation of multiple classes of V0 neurons in zebrafish spinal cord: progenitor heterogeneity and temporal control of neuronal diversity. *J. Neurosci.* **32**, 1771-1783.
Schmitt, E. A. and Dowling, J. E. (1999). Early retinal development in the zebrafish, *Danio rerio*: light and electron microscopic analyses. *J. Comp. Neurol.* **404**, 515-536.
Smear, M. C., Tao, H. W., Staub, W., Orger, M. B., Gosse, N. J., Liu, Y., Takahashi, K., Poo, M. M. and Baier, H. (2007). Vesicular glutamate transport at a central synapse limits the acuity of visual perception in zebrafish. *Neuron* **53**, 65-77.
Snyder, J. B., Nelson, M. E., Burdick, J. W. and Maciver, M. A. (2007). Omnidirectional sensory and motor volumes in electric fish. *PLoS Biol.* **5**, e301.
Stein, B. E. and Clamann, H. P. (1981). Control of pinna movements and sensorimotor register in cat superior colliculus. *Brain Behav. Evol.* **19**, 180-192.
Stein, B. E., Magalhães-Castro, B. and Kruger, L. (1976). Relationship between visual and tactile representations in cat superior colliculus. *J. Neurophysiol.* **39**, 401-419.
Stuermer, C. A. (1988). Retinotopic organization of the developing retinotectal projection in the zebrafish embryo. *J. Neurosci.* **8**, 4513-4530.
Torres, B., Luque, M. A., Pérez-Pérez, M. P. and Herrero, L. (2005). Visual orienting response in goldfish: a multidisciplinary study. *Brain Res. Bull.* **66**, 376-380.
Valentine, D. E. and Moss, C. F. (1997). Spatially selective auditory responses in the superior colliculus of the echolocating bat. *J. Neurosci.* **17**, 1720-1733.
Yokogawa, T., Hannan, M. C. and Burgess, H. A. (2012). The dorsal raphe modulates sensory responsiveness during arousal in zebrafish. *J. Neurosci.* **32**, 15205-15215.
Zhu, P., Narita, Y., Bundschuh, S. T., Fajardo, O., Schärer, Y. P., Chattopadhyaya, B., Bouldoires, E. A., Stepien, A. E., Deisseroth, K., Arber, S. et al. (2009). Optogenetic dissection of neuronal circuits in zebrafish using viral gene transfer and the tet system. *Front. Neural Circuits* **3**, 21.

Movie 1. Zebrafish larva ignores paramecia in the dark. Video of a larval zebrafish surrounded by paramecia in dark behavioral testing conditions. No attempt to capture paramecia is made, despite their close proximity. This 4 s behavioral video was recorded at 60 frames s^{-1} and is played back at 20 frames s^{-1} (3× speed reduction). Scale is 97 pixels mm^{-1}.

Movie 2. The same zebrafish larva in lit conditions captures a paramecium. Video of the larval zebrafish from supplementary material Movie 1 demonstrating it can detect a relatively distant paramecium and perform prey capture, but only after it has been accommodated to the light. This 2 s behavioral video was recorded at 250 frames s^{-1} and is played back at 20 frames s^{-1} (12.5× speed reduction). Scale is 97 pixels mm^{-1}.